2017

Development of an Integrated Thermal Energy Storage and Free-Piston Stirling Generator for a Concentrating Solar Power System

Songgang Qiu

Laura Solomon

Garrett Rinker

energies

MDPI

Article

Development of an Integrated Thermal Energy Storage and Free-Piston Stirling Generator for a Concentrating Solar Power System

Songgang Qiu *, Laura Solomon and Garrett Rinker

Department of Mechanical and Aerospace Engineering, Benjamin M. Statler College of Engineering and Mineral Resources, West Virginia University, Morgantown, WV 26506, USA; laura.solomon@mail.wvu.edu (L.S.); grinker@mix.wvu.edu (G.R.)

* Correspondence: songgang.qiu@mail.wvu.edu; Tel.: +1-304-293-3342

Academic Editor: K.T. Chau

Received: 22 August 2017; Accepted: 4 September 2017; Published: 8 September 2017

Abstract: Incorporating thermal energy storage (TES) into a concentrating solar power (CSP) system extends the power production hours, eliminating intermittency and reducing the Levelized Cost of the Energy (LCOE). The designed TES system was integrated with a 3 kW free-piston Stirling convertor. A NaF–NaCl eutectic salt was chosen as the phase change material (PCM) with a melting temperature of 680 °C. This eutectic salt has an energy density that is 5 to 10 times that of a typical molten salt PCM. In order to overcome the drawbacks of the material having a low thermal conductivity, heat pipes were embedded into the PCM to enhance the heat transfer rate within the system. Since the dish collector tracks the sun over the course of the day, two operational extremes were tested on the system; horizontal (zero solar elevation at sunrise/sunset) and vertical (solar noon). Although the system's performance was below the expectations due to improperly sized wicks in the secondary heat pipes, the results indicated that the Stirling engine was able to produce 1.3 kWh of electricity by extracting latent heat energy from the PCM; thus, the concept of the design was validated.

Keywords: phase change material (PCM); thermal energy storage (TES); concentrating solar power (CSP); heat pipe

1. Introduction

There has been a marked increase in research into renewable and alternatives to fossil fuel-based power generation resulting from their ever dwindling supply and their environmental impact. The biggest challenge limiting their widespread use is the inherently transient nature of most renewable resources. Since electrical energy cannot be stored cost effectively in large scale, it is often converted into mechanical, chemical, or thermal energy in order to store excess energy. However, these conversions typically add conversion losses. A solar thermal power plant is a good example of efficient energy conversion and storage. In a concentrating solar power (CSP) plant, incoming solar radiation is focused on a small receiving area and used to increase the temperature of the working fluid of a thermal power generation cycle. As the solar energy is being used in the form of heat, it allows for the easy integration of thermal energy storage (TES) without the costly energy conversion processes encountered with other renewable resources. Additionally, while CSP plants are the primary example application of TES, it can have a significant impact on many other fields, such as in industrial cooling applications.

TES can be broken down into three categories based on the principle behind the means of energy storage. The first form of TES is sensible heat storage, where a material stores (releases) energy by raising (lowering) its temperature without changing the material's phase or state. In contrast, latent heat TES takes advantage of the large quantities of energy required to change the state of a material,

whether it is a solid–liquid, solid–gas, or liquid–gas transition. As latent heat-based TES systems have higher energy densities, they require a smaller amount of the storage material in comparison to sensible heat TES systems, thus resulting in a reduction of system size and cost. Another form of TES is thermochemical-based storage, which utilizes reversible exothermic/endothermic reactions to store/release energy. Although thermochemical-based storage offers the highest energy density, its development is still in the early stages [1]. Currently, the majority of TES that has been implemented in operational CSP plants have been in the form of large molten salt-based sensible heat storage systems in either parabolic trough or central receiver-type plants [2–4]. These systems are relatively inefficient, with typical solar to electric efficiencies of 15–20%; they require complex pumping systems, and have a large overall system size for installation at plant sizes of tens or hundreds of MW. Additionally, the system must be well insulated to prevent the molten salt from freezing that would result in a total system shut down.

Of the four types of state changes, the solid–liquid phase change is the most promising for use in latent heat-based TES due to its reasonably high heat of fusion and relatively small volumetric changes. A wide range of materials has been investigated as potential phase change materials (PCMs), including paraffin wax, fatty acids, sodium nitrate, potassium nitrate, sodium nitrate–potassium nitrate eutectics, sodium chloride, and sodium borate oxides [2,5–7]. Nevertheless, the use of PCMs is not without its own unique difficulties and challenges. Most prominently is the low thermal conductivity of the studied materials, particularly in the solid phase, which has a limiting effect on the heat transfer during the discharging process. Numerous methods of improving the heat transfer rate have been studied, including adding a highly conductive material to the PCM [8–13], employing multiple PCMs with varying melting temperature [14–16], macro- and micro-encapsulation [5,6,17–25], and embedding fins into the PCM [26–29]. Another option is to use heat pipes. Heat pipes are efficient, simple, and reliable. They have no moving parts and can transfer heat at high rates over long distances at nearly isothermal conditions, which make them ideal for use in TES applications.

Several experimental and numerical investigations into using heat pipes for TES at CSP plants have been conducted [30,31]. Sharifi et al. [32] compared the melting rate of a vertical cylindrical PCM heated by a rod or heat pipe at the center of the PCM, and their results show that the use of heat pipes resulted in a higher melting rate. Motahar and Khodabandeh [33] reported improvements in the melting and solidification rates of a cylindrical PCM by utilizing heat pipes. An increase of 70% for the melting rate of a PCM with embedded heat pipes was reported by Robak et al. [34]. Shabgard et al. [35] investigated the impact of heat pipes on two configurations of PCM-based TES; one where the PCM surrounds tubes through which the heat transfer fluid (HTF) flows, and the second where the HTF cross-flows over tubes of encapsulated PCM. Their work showed that heat pipes have a more significant impact when the PCM is in the tubes rather than surrounding them. In a related work, Shabgard et al. [15] numerically studied a cascaded multi-PCM system with gravity-assisted heat pipes embedded into the PCM using a thermal element network approach. Their results indicated that 10% more exergy can be recovered during a 24-h charging/discharging cycle in comparison to a non-cascaded system. Tiari et al. [36–38] numerically studied the charging and discharging of a TES system that used KNO_3 as the PCM to determine the influence that several key parameters, such as heat pipe spacing, fin length, and fin pitch, had on the charging and discharging rates. Hays et al. [39] investigated the use of heat pipes to improve the thermal conductivity of a wax-based PCM for small-scale energy storage in conjunction with a thermoelectric generator, and their results indicated a thermal conductivity of 8.23 W/mK, which is a vast improvement from the baseline 0.5 W/mK of pure PCM without heat pipes.

While the above work is for generic PCM TES systems, some studies have been conducted on storage systems that are integrated into a dish-Stirling CSP plant. Shabgard et al. [40] investigated the use of a heat pipe PCM TES system for use in a dish-Stirling system where the PCM acts as a thermal buffer to alleviate transients in solar insolation. Sharifi et al. [41] examined a system that had a single heat pipe that was used for both charging and discharging of the PCM for a dish-Stirling receiver.

In a system considered by Cui et al. [42], a heat pipe is directly irradiated and transfers the energy to the PCM and heater head. They noticed a marked improvement in the performance of the receiver and a reduction in the temporal temperature variations along with a reduction in the overall weight of the system. Mahdavi et al. [43–45] analyzed the performance of a complex heat pipe network in a dish-Stirling system where the primary heat pipe is used to deliver the solar radiation to the Stirling heater head and an array of secondary heat pipes are used to transfer the excess energy to the PCM for storage.

Numerous positive performance enhancements can be expected by integrating a heat pipe network-based TES module with a dish-Stirling system. Besides the increase of charging and discharging rates due to improved heat transfer, the energy output of each individual TES unit is also increased, as a larger dish can be used to allow for simultaneous power production and energy storage during peak solar insolation. A directly integrated storage system will not have the same hot liquid pumping drawbacks of a large centralized storage system. This will lead to a reduction in the levelized cost of energy (LCOE) associated with the CSP plant. Additionally, as a dish-Stirling-type CSP is a distributed generation plant, if a failure was to occur with one of the TES modules or engines it would only affect that unit and the remainder of the solar field could continue to generate the required electrical power. Further cost reductions are feasible as the heat pipe transport system delivers heat uniformly to engine's heater head, allowing for a lower optical accuracy of the concentrator. This not only reduces the cost of the concentrator but also the chassis, tracking drive, Stirling engine receiver, and various other subsystems. Lastly, the overall efficiency is increased as the heat is uniformly delivered to the engine's heat accepter, leading to operation at a higher average hot end temperature without the development of hot spots that would lead to material failure.

The proposed heat pipe-based TES system is to be incorporated onto the heater head of a free-piston Stirling engine that is at the focal point of a dish-type solar collector. The incoming solar radiation that enters the receiver is conducted to the PCM by the heat pipe array. The chosen PCM is required to have a melting temperature in the optimal operating range of the engine, between 600 and 700 °C. During off-sun operation, the same heat pipe network transfers energy from the PCM to the engine's heater head. Both the free-piston Stirling engine and the TES module are hermetically sealed and maintenance-free. Additionally, the system is a passive heat transport system; thus, it requires no pumps, fittings, or other components to transport high-temperature molten salt. Furthermore, the system is not affected by ambient temperature levels or by various melt–freeze cycles. The integration of TES to the free-piston Stirling engine system allows for electricity to be generated during solar transients and non-daylight hours. The TES system was designed to have sufficient storage to supply the required thermal energy for 1 h of operation at an average output of 3 kW_e. This will allow for a significant reduction in LCOE associated with the free-piston Stirling dish convertor. The goal of this project is to develop a PCM-based TES unit that can be integrated with a free-piston Stirling engine for a CSP system to reduce the LCOE. The novelty of the design is: (1) a complete passive TES system that does not require a pump loop to circulate the molten salt, therefore the system reliability is increased while the maintenance cost is reduced; and (2) an innovative configuration of the heat pipe network that can ensure simultaneous engine power production and PCM charging.

2. System Design

2.1. Eutectic Salt Selection

A latent heat-based TES system has a higher specific weight and volume in comparison to a sensible heat-based system. This makes its integration into a Stirling dish system (PowerDish™, Infinia Corporation, Kennewick, WA, USA) more practical. There are numerous materials that can be used as a PCM: a promising choice is a eutectic mixture of alkali halides with attractive properties for use in TES. The main criterion for choosing a PCM is that the material has a melting temperature within the desired operating temperature range. For the designed system using the Infinia 3 kW free-piston

Stirling engine, the chosen PCM should have a melting point between 600 and 700 °C so as to ensure that energy is supplied to the engine at the temperature required for the system to operate at peak efficiency. A NaF–NaCl eutectic (34% mol. NaF) mixture with a melting point of 680 °C was chosen for use as the PCM. This allows for the Stirling engine to operate for an extended period of time using the latent heat of fusion near the melting point. Additionally, a comparable amount of solid and liquid sensible energy can be extracted over the wider operational range of roughly 750–300 °C. Although the conversion efficiency of the Stirling converter decreases as the temperature decreases, the system will generate useful electricity continuously, even down to the lower bound of the operating temperature due to the outstanding turn down ratio of Stirling engine generators. The effective surface of the PowerDish™ concentrator (PowerDish™, Infinia Corporation, Kennewick, WA, USA) to be used for the project has an area of 14.8 m^2, which can provide 12.58 kW of solar energy to the system assuming 850 W/m^2 direct normalized insolation (DNI).

2.2. TES Module Support

The TES container was welded to a support ring that was brazed to the Stirling engine heater head. The support of the TES was designed using flexure springs that are compliant in the axial direction to allow for the motion of the casing and thermal expansion while being laterally rigid so as to prevent sagging due to gravitational effects. In this specific design, the flexures are attached directly to the TES container, resulting in a significant thermal gradient over the flexure. As this can result in high thermal stresses, the flexures were optimized such that they did not exceed the material endurance limit of the flexure. The details of the TES flexure design process are presented by the authors in a separate paper. The typical temperature distribution and stress field are shown in Figure 1.

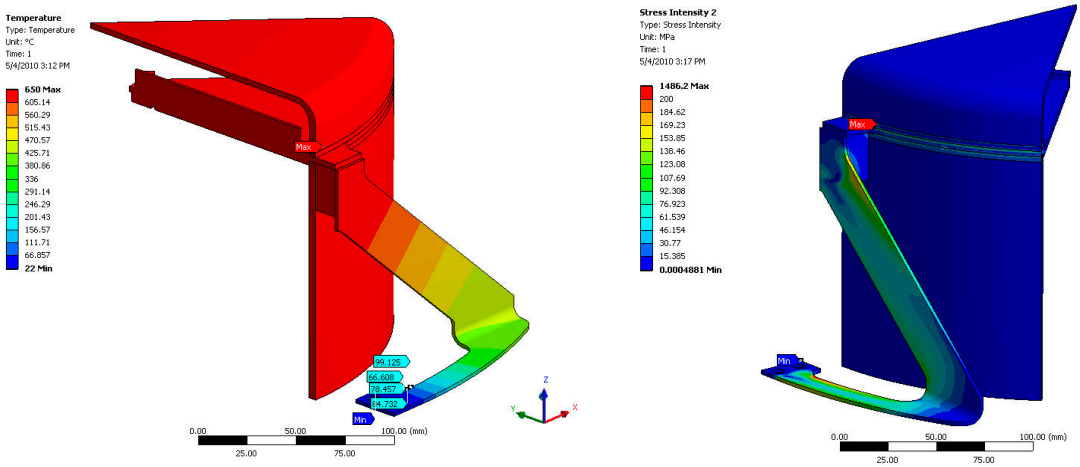

Figure 1. Temperature distribution (**left**) and stress field (**right**) within the designed thermal energy storage (TES) flexure.

2.3. TES Module Design

The prototype TES free-piston Stirling engine is shown in Figure 2. The heater head of the 3 kW engine acts as the condenser of the primary heat pipe that transfers the incoming solar energy to both the Stirling engine and the PCM storage material. The secondary heat pipes are embedded into the NaF–NaCl eutectic PCM salt. The system also consists of a receiver vapor chamber that acts as the evaporator of the central primary heat pipe, the TES container and Stirling engine supporting flexures, and the flexure support frames. The diameter of the Stirling engine and the linear alternator is 203 mm and 260 mm, respectively. The engine and alternator have a combined length of 533 mm. The TES module is 424 mm long with a 300 mm diameter.

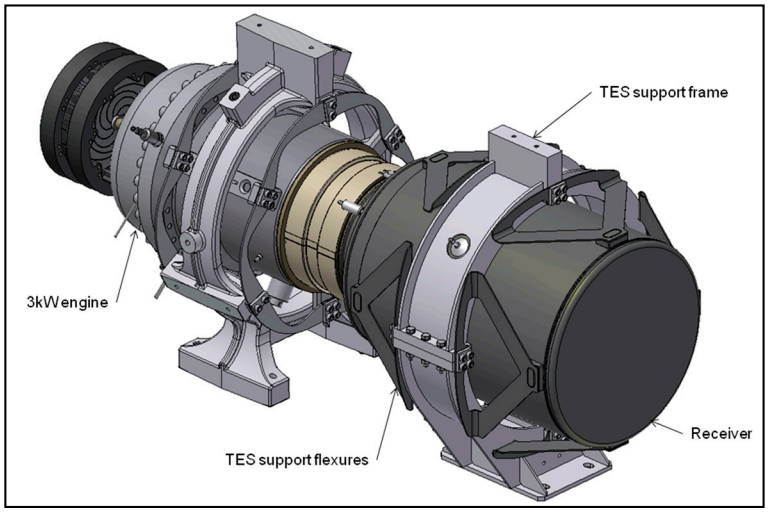

Figure 2. Stirling engine and TES module assembly.

A schematic of the TES module for both the charging and discharging process is shown in Figure 3. The yellow region is the heat pipe working fluid, the gray color denotes the NaF–NaCl PCM, and the red arrows indicate the direction of the heat flow. During charging, solar energy is absorbed by the TES receiver face on the left in Figure 3. This causes the sodium in the heat pipe in contact with the receiver to evaporate and move towards the Stirling engine heater head/heat accepter, on the right in Figure 3. The sodium then condenses, thus transferring the thermal energy to both the Stirling engine and the PCM. The Stirling engine absorbs the majority of the incoming thermal energy, while the excess thermal energy is routed to the PCM by an array of 32 embedded heat pipes that have a 12.7 mm diameter. During discharging, the energy stored in the PCM is extracted and transferred to the Stirling engine via secondary heat pipes as depicted in Figure 3. In discharging mode, the secondary heat pipes act as the evaporator while during charging they function as a condenser section.

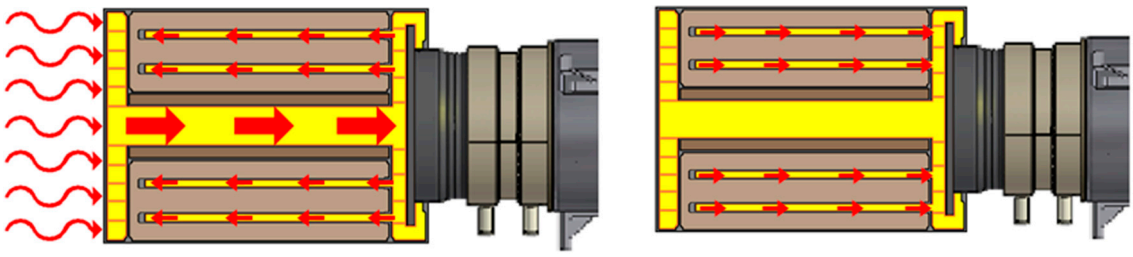

Figure 3. TES module schematic for charging (**left**) and discharging (**right**) mode.

A detailed design analysis was conducted on the TES module prior to the start of testing. In particular, the heat transfer limit was determined according to the design capacity at the targeted operating temperature. The capillary pressure limit of the wick and the sonic limit of the vapor in a pipe determine the heat transfer limit. The nominal heat rate supplied by the concentrator dish during on-sun operation is about 12 kW. This heat is distributed over the 30 cm diameter evaporator receiver surface. The following limiting cases were examined during the wick analysis: (1) gravity-neutral horizontal charging, Figure 4a; (2) mid-day vertical charging that is adverse gravity for the secondary heat pipe but gravity-aided for the primary heat pipe, Figure 4b; and (3) gravity-aided operation of the secondary heat pipes during discharging (vertical with the dish pointing down), Figure 4c.

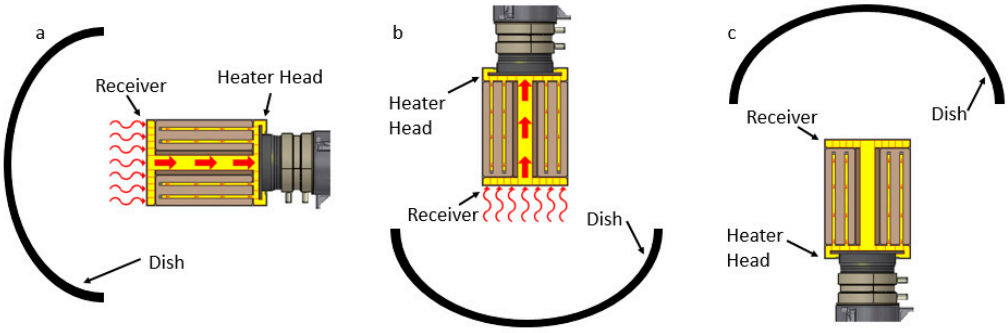

Figure 4. TES module orientations studied: (**a**) gravity-neutral horizontal charging; (**b**) mid-day vertical charging (adverse gravity for the secondary heat pipes and gravity-aided for the primary heat pipe), and (**c**) gravity aided discharging of the secondary heat pipes with the dish pointing downwards.

The analysis results of the gravity-neutral charging case showed that the capillary pressure is adequate for the condensed sodium to return into the heat pipes. For mid-day operation mode, the module's vertical orientation allows for the condensed sodium to return to the primary heat pipe evaporator via gravity and therefore the wicking is not required. However, in the secondary heat pipes, the condensate must travel through the entire length of the pipe against gravity to arrive at the central heat pipe and then to the primary evaporator. A graphic of an finite element method (FEM) analysis showing the heat pipe array is depicted in Figure 5, the result of which is a required maximum capillary pressure of 2140 Pa, compared to 3100 Pa available from the selected wick. Thus, the secondary heat pipes will function well in this extreme orientation.

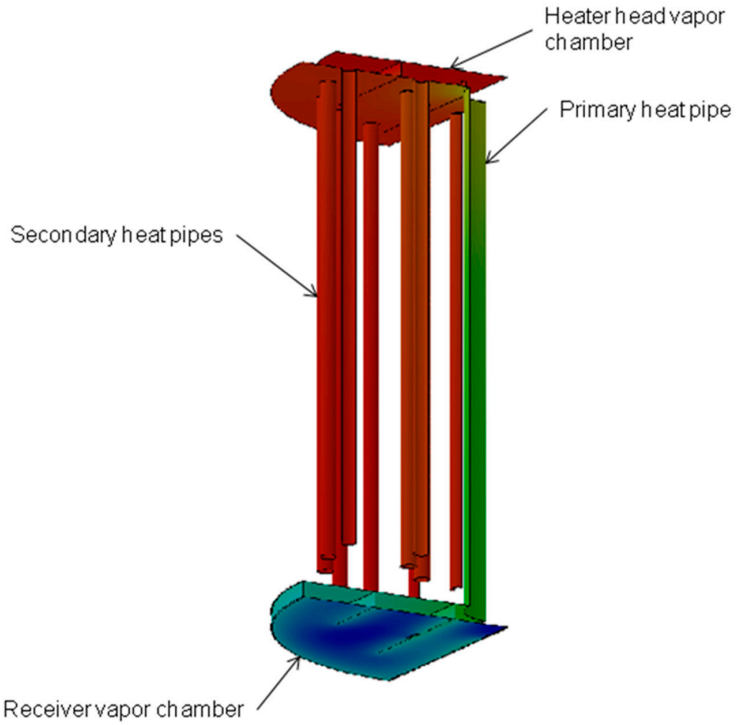

Figure 5. Wick finite element method (FEM) Analysis.

For discharging, the Stirling engine and TES module will be vertically orientated; however, unlike during mid-day operation, the dish will point towards the ground, allowing the PCM to solidify and shrink (Figure 4c). The voids will form near the receiver end. The secondary heat pipes are under adverse gravity again.

The integrity of the TES container was thoroughly analyzed using structural analysis. The primary focus of the structural analysis was for the cold startup case, where the engine begins electricity generation in the morning. The entire TES structure and the PCM are at ambient temperature during engine startup. When the receiver is brought on-sun, its temperature increases rapidly and thermal expansion will take place, which results in high thermal stresses. A temperature of 650 °C was applied to the TES vessel, while the flexure attachments were held to 22 °C. In addition, it was assumed that the 3 kW engine was also at 22 °C, with a thermal gradient along the heater head. These conditions represent a worst-case scenario for the temperature distribution in the engine/TES system. The temperature field of the integrated TES and engine is shown in Figure 6 below. In addition to this thermal load, the weight of the engine and the TES module were applied when the system is oriented to the horizontal. The stress analysis indicates that the combined effects of the thermal expansion and the TES/Engine weight are within design stress ranges allowable for the TES and Stirling engine materials. The allowable stress ranges used are from the ASME pressure vessel code. The contour plot of system stress distribution is shown in Figure 7.

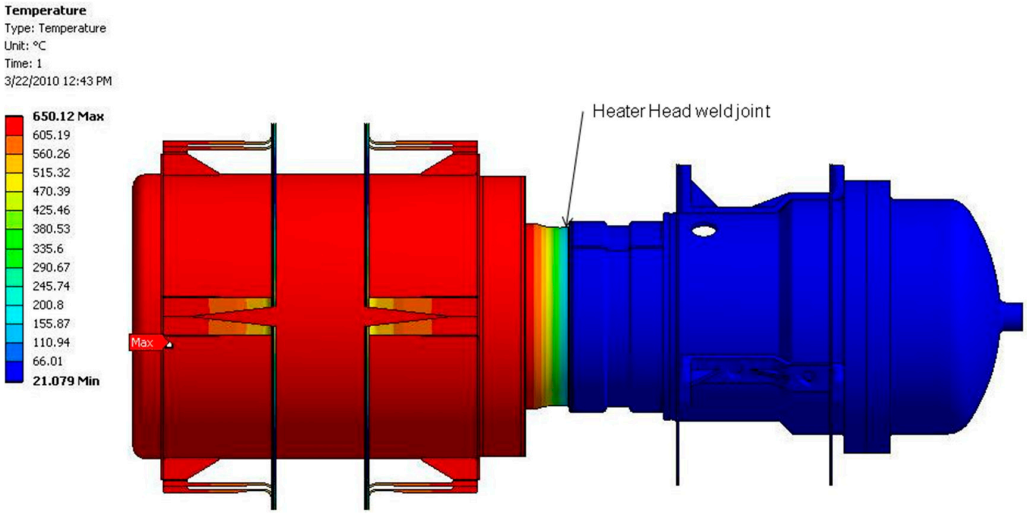

Figure 6. Temperature Field in Engine/TES System.

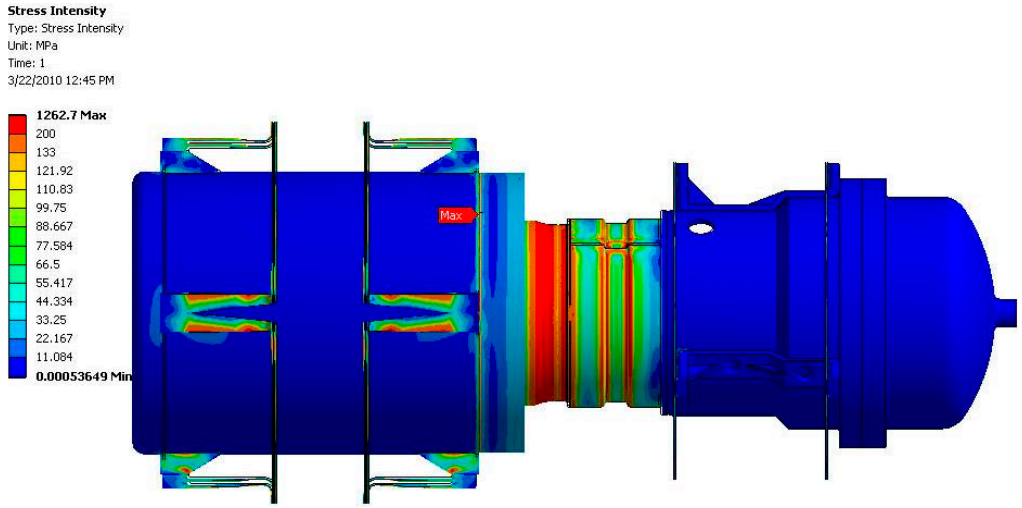

Figure 7. Stress distribution in engine/TES System.

The results of the stress analysis provide the basis for the system control algorithm that can be used to vary the heating rate to the receiver such that material stresses will remain below the limits. Thermocouples were installed on the TES module surface at strategic locations to capture real-time temperatures that are monitored and employed for the control algorithm. The thermal loading of the TES vessel was examined using Ansys structural models to investigate the effect of various heating rates on the stress field within the structure. Numerous transient analyses were conducted where the temperature at predetermined probe locations was recorded along with the resulting stresses. Additional laboratory testing verified that the thermal stresses induced during a cold startup could be managed by temperature measurement and varying the heating rate to the receiver via the developed protocols.

3. LCOE Analysis

An LCOE analysis was performed to determine the impact of the TES module on the existing 3 kW dish-Stirling CSP system. Ricardo North America, an engineering consulting firm, was brought in to perform the cost analysis of the parts and assemblies. For the production scale of 40,000 TES modules per year, the estimated LCOE for the integrated dish-Stirling-TES CSP system is 16.19 ¢/kWh. This preliminary LCOE analysis was conducted by using a modified form of NREL's system advisor model (SAM) and the third party part cost. Although the estimated LCOE is higher than the current goal set forth by the SunShot inventive, the LCOE can be lowered further through design refinement, replacing high-cost materials, and reducing the assembly cost.

4. Testing of the Dish-Stirling TES CSP System

An induction heater with a ceramic susceptor was used to emulate the incoming solar radiation for the laboratory testing of the dish-Stirling-TES CSP system. Laboratory testing was carried out in two phases. The TES module was charged then discharged while the Stirling engine was not in operation during Phase I. For Phase II, the Stirling engine was fully operational. In Phase I, to prevent the excessive thermal stresses during a cold startup, the heat flux protocol devised based on the finite element analysis (FEA) was used to heat the TES receiver. The TES module was monitored for the temperature difference at various points. The output of the induction heater was adjusted to keep the temperature differences under the predefined threshold. The TES module alone was charged and discharged a few cycles before the Stirling engine was filled up with working fluid (helium), and Phase II testing was conducted with the Stirling engine fully operational. The TES receiver was heated up in accordance with the heating profile developed during Phase I testing, and electricity was generated by the Stirling convertor.

K-type thermocouples were used to measure the temperature of the TES module. The container was outfitted with 24 thermocouples placed on the exterior of the PCM salt container according to the schematic shown in Figure 8. Thermocouples 1 to 6 were located axially along the module. At each of these six axial locations, four thermocouples were radially mounted, labeled A through D in Figure 8. Thus, the locations of the thermocouples are referred to as A1, A2, A3, A4, A5 and A6; B1, B2, B3, B4, B5 and B6; and so on. The temperature gradients on the heat pipe vapor chamber (solar receiver) were measured with the first four axial thermocouples. The temperature of the PCM was measured via thermocouple 5 that was placed at the midplane between the Stirling engine and the receiver. When the four radial thermocouples at axial location 5 reach a temperature of 750 °C, it is assured that all of the PCM has undergone a complete phase change and is now entirely molten. Thermocouple 6 at the final axial location measures the temperature of the condenser attached to the Stirling heater head.

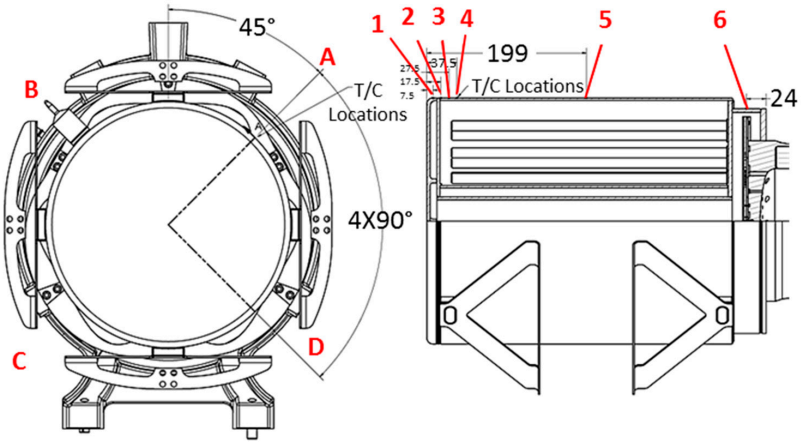

Figure 8. Radial and axial location of thermocouples.

The FEA results showed that at any radial location, the measured temperature difference in between thermocouples 1 and 4 has to stay under 100 °C to prevent large thermal gradients from inducing high thermal stresses. During heating, the set point of the induction heater was raised gradually to ensure that the temperature difference stayed below the 100 °C threshold. The control thermocouple of the induction heater was also installed at axial location 1, which is close to the receiver surface that is being heated. For a properly designed heat pipe, it is nearly isothermal along the length between the evaporator and condenser, the difference between axial thermocouple location 1 and 6 should be small. Note that due to a heat pipe operating principle, heat pipes only operate isothermally once they reach their effective operating temperature and the sodium working fluid evaporation rate reaches the design point. For the chosen heat pipe used in this work this occurs at around 600 °C. A data acquisition system (DAQ) equipped with LabVIEW (LabVIEW V8.0, National Instruments, Austin, TX, USA) virtual instrument (VI) software was connected to the TES module to monitor and record the power, temperatures, and susceptor parameters. This DAQ system was also employed to manage the induction heater power input for the regulation of heater head temperature and the control of engine stroke. The TES module in the testing rig with the induction heater and other instrumentation attached is shown in Figure 9. The operating conditions of the integrated TES-dish-Stirling CSP system are listed in Table 1. The uncertainties in the measurements originate from the thermocouples and power meter. The thermocouples have an accuracy of 0.4% or ±2.8 °C, while the power meter has an uncertainty of 0.1%.

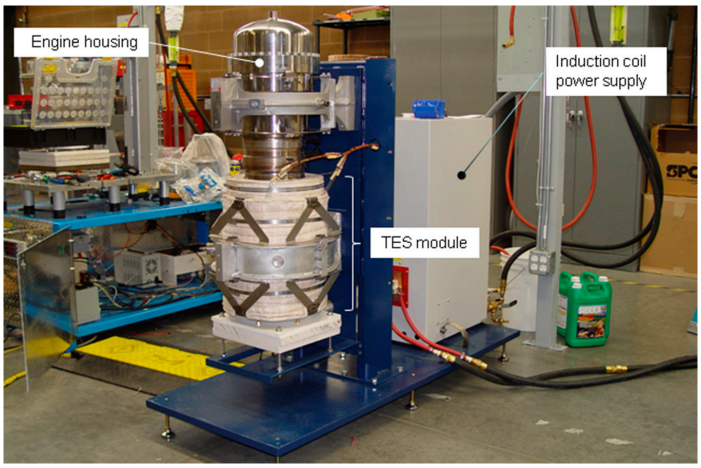

Figure 9. *Cont.*

Figure 9. TES module test stand with induction heater (**top**) and TES module with heat tape and instrumentation attached (**bottom**).

Table 1. Operating Conditions.

Parameter	Operating Condition
Engine nominal operating temperature	650 °C
Rejection temperature	45 °C
Operation pressure (Engine)	40 bar
TES testing temperature	450–700 °C

4.1. Gravity-Assisted Results

Figure 10 shows the measured temperature data for Phase I testing. The temperatures of the test results are represented by thermocouples located at radial position "A". Figure 10 also shows the duty cycle of the susceptor. Although the duty cycle cannot be directly used to determine the power input levels, the input power levels can be estimated based on correlations developed during the previous testing of the Stirling engine alone. Note that the TES module was heated overnight at 300 °C to prevent any of the sodium within the heat pipes from solidifying and impairing their function. It can be seen from Figure 10 that once the receiver temperature reaches approximately 550 °C, heat transfer to the Stirling engine's heater head starts. It is evidenced by the rapid increase of the temperature in thermocouple 6. It was anticipated that the temperature difference between thermocouples 3 and 6 would be small once the optimal temperature of the evaporator (550–600 °C) was reached, as the heat pipe should be operating at near isothermal conditions. However, the 350–400 °C temperature difference between thermocouple 3 and 6 indicates that the heat pipes were improperly functioning. The 11 kW of thermal energy into the central heat pipe was split between the Stirling engine and the PCM. The heat pipes that were embedded into the PCM were sized based on the anticipated 3 kW of heat while the remaining 8 kW was being directly transferred to the Stirling engine. Therefore, the system was not capable of transferring the full 11 kW to the PCM only. It was determined to move on to TES testing with the Stirling engine running.

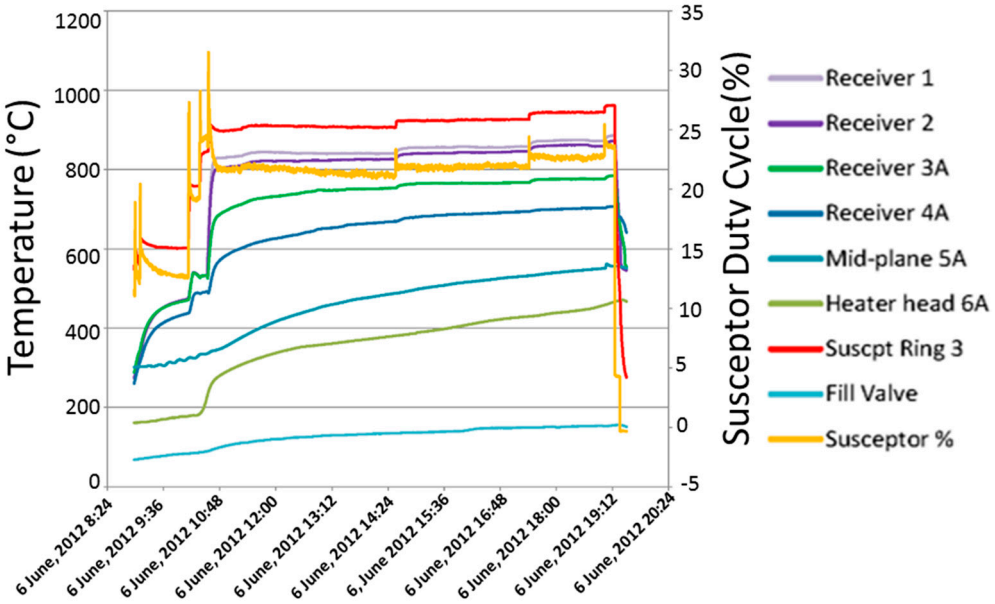

Figure 10. Temperature data from Phase I testing.

Figure 11 shows the temperature and susceptor duty cycle results from Phase II testing. The heat pipe starts transferring heat from the receiver to the Stirling engine's heater head when the receiver reaches 550–600 °C. This is indicated by the temperature increase of thermocouple 6. The divergence between the thermocouple at the receiver and the thermocouple(s) at axial position 3 is of particular interest. It occurs when the receiver temperature reaches 550–600 °C, activating the heat pipe to function. For a properly operating heat pipe, the temperature difference should be very small. When the temperature of the evaporator is sufficiently high, the increased sodium vapor pressure forces the sodium vapor to travel down the heat pipe to the lower temperature and low pressure condenser. The temperature divergence indicates that the condensed sodium is unable to return to the evaporator surface rapidly enough, resulting in an increase of the temperature within the evaporator section. Prior to the heat pipe activation temperature, the temperature of the Stirling engine's heat receiver was actually high enough that the Stirling engine started. The stroke of the engine piston was initially kept to a minimum level until the heat pipe condenser and engine heat accepter temperature began to increase owing to the heat pipe beginning to operate. At this point, the piston stroke was increased, resulting in a spike in power output that decreased rapidly back down to the previous output level. The engine stroke was increased two more times with the same results before being returned to the minimum engine stroke. This action temporarily suppressed the heat pipe condenser temperature as one would expect, but it also trigged a small short-term temperature spike in the receiver at thermocouple locations 1 and 3, suggesting a deficit in the sodium condensate return, since as the Stirling engine absorbs more heat, more sodium vapor mass is required to sustain the energy transfer. After the sodium vapor condenses on the condenser surface, the condensate has to find the way back to the central heat pipe to replenish the primary evaporator. For the primary heat pipe this was a gravity-aided situation, meaning that the liquid condensate should return to the evaporator due to gravitation effects and the differences in the respective densities of the liquid and vapor sodium. However, it is likely that a portion of the condensed sodium found its way to the embedded secondary heat pipes instead of returning to the evaporator.

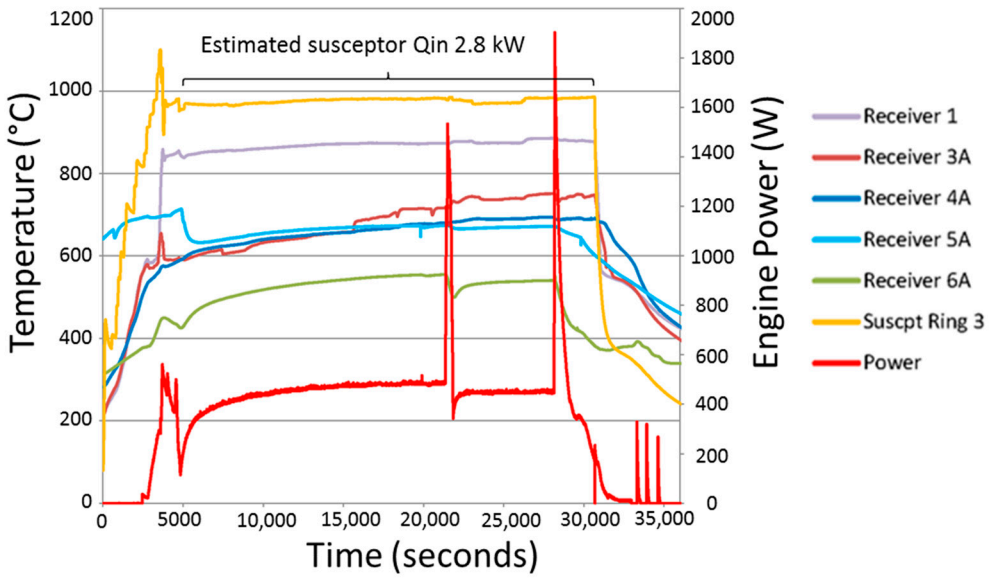

Figure 11. Temperature data and engine power from Phase II testing.

The temperatures within the system increased gradually until it reached thermal equilibrium. The spikes of the engine power seen in Figure 11 are due to controlled stroke variation. The increase in the engine power output results in a slight temperature increase at thermocouple locations 1, 3, and 4 on or near the receiver. This also supports the notion that the return of sodium condensate may have been hinded. The engine stroke was then set back to the minimum value for rapid TES charging. The engine was controlled to full stroke after it recovered from the previous stroke variation, and then operated at full stroke for the rest of the test. After a peak output of 1.9 kW, the engine power stabilized to around 350 W and the receiver temperature decreased slightly. Shortly after commanding full stroke, part of the power to the receiver was turned off, causing the power output to drop immediately and the temperature at thermocouple location 5 to decrease. This indicates that the engine was drawing energy out of the PCM. The power to the susceptor was turned off once the engine power dropped below 200 W, after which the system continued to operate for a short period of time on the remaining stored thermal energy with engine power continuously decreasing until the engine stopped. The spikes in power output after this are a result of the engine self-starting due to the thermal energy that was built up within the heater head.

4.2. Horizontal Orientation Testing

In order to investigate the influence of orientation on the performance of the heat pipe network, a horizontal test was conducted. The reasoning behind this is that if the lack of performance during the previous testing was due to sodium condensate in the secondary heat pipe being unable to return to the primary evaporator because the heat pipe wick could not provide sufficient capillary pressure to overcome the frictional force and adverse gravity, the horizontal orientation is gravity-neutral so it would be easier for the condensate to travel back to the evaporator. Figure 12 shows the experimental results of the TES module. The TES module was outfitted with additional heaters and was heated to around 750 °C so that the chosen NaF–NaCl eutectic salt was at a superheated liquid state. In the horizontal gravity-neutral orientation, the receiver was able to accept significantly higher heat than in the vertical orientation. An estimated 5.7 kW was generated by the susceptor at a skin temperature of 800 °C as compared to 3 kW in the vertical tests. Additionally, the secondary heat pipe array was able to more effectively transfer heat into the PCM in the horizontal orientation than in the vertical gravity-adverse orientation that was previously tested. Note that the random decreasing output of the susceptor was a result of the VI losing the set point.

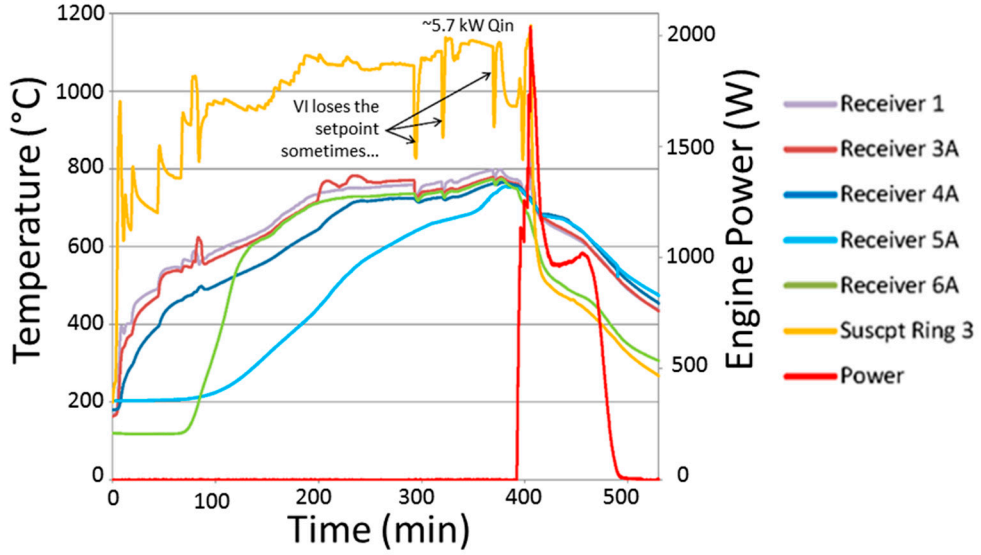

Figure 12. Horizontal TES testing results. VI: virtual instrument.

After approximately 390 min, the desired temperature within the PCM was reached. The engine was then charged with helium incrementally to the desired operating pressure, at which point the power to the susceptor was shut off and the engine started extracting power from the PCM alone. The engine's power initially spiked to 2 kW before it began to rapidly decrease. In this test, the engine power stabilized at around 1 kW as the engine extracted the stored thermal energy from the PCM, as compared to 400 W in the vertically orientated test and the susceptor was continuously on. These results are shown in Figure 13. The total electrical energy generated during the course of the experiment was roughly 1.3 kWh before the engine stopped. This is an improvement over the 400 W seen in the vertical test.

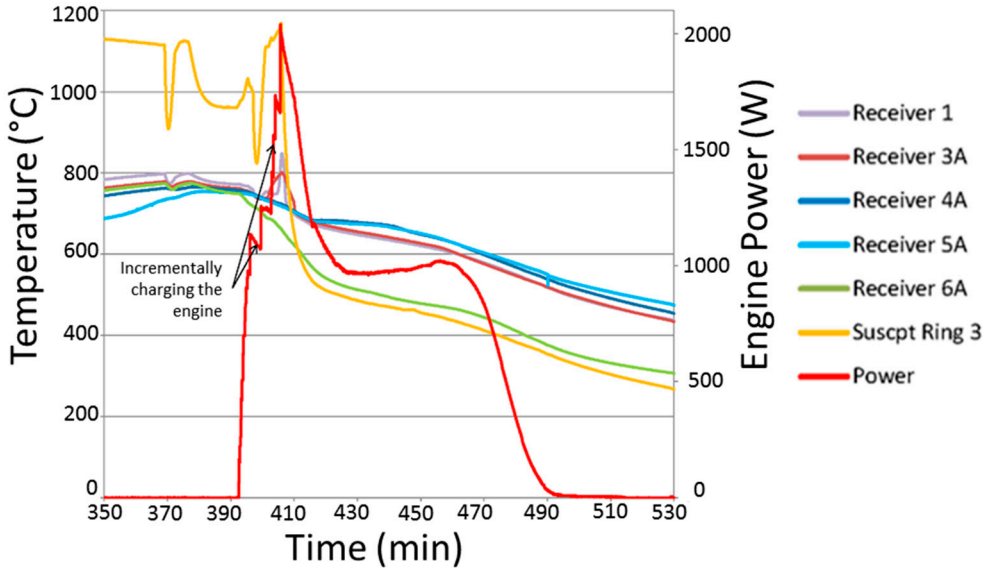

Figure 13. Temperatures during discharging in the horizontal orientation.

The comparison between the vertically oriented test and the horizontal orientation test indicates that in the current design, the capillary force of the wick in the secondary heat pipes is inadequate to return the sodium condensate to the receiver. In both tests, the overall performance of the system was limited by the performance of the heat pipe network. A further review of the results and design

analyses show that the wick sizes were inappropriate. However, it is still promising that the power output was relatively flat during the PCM solidification process. This is a good indication that the heat pipe network was capable of extracting energy from the PCM during the discharging process despite the low thermal conductivity of the material in the solid phase. The heat extraction capability of the heat pipes can be improved by proper design refinements and a thorough design analysis. At the time of this system design, the heat pipe analysis was performed using conventional analysis techniques. Wick selection is a balance of capillary action and permeability, both of which are related to the pore radius of the wick material. A smaller pore size radius equates to higher capillary action and this higher "pumping power", whereas a larger pore radius equates to higher permeability and therefore lower viscous losses. A sintered nickel powder was selected for this design, which had a flux capacity greater than 100 W/cm^2. The heat pipe size was chosen based on the sonic limit at the designed heat input for a given operating temperature. It was apparent that the conventional analysis was not sufficient. The authors have developed a new computational fluid dynamics (CFD) modeling method that is applicable for both a complex heat pipe network as in this paper and the conventional heat pipes. The CFD model was validated by the experiment testing data, [43–45]. It was determined that the geometry, size, and locations of the secondary heat pipes have a significant impact on the performance of the system. The spacing of the primary condenser and the exit geometry of the secondary to the primary condenser affect the sodium vapor jetting, and hence the flow distribution and heat transfer. The heat pipe design method is still under development. The hardware demonstration is planned at the sub-scale level before moving onto full-scale system demonstration. The new heat pipe design will be optimized to provide a smooth vapor flow transition from the secondary heat pipes to the primary condenser and to contain sufficient margin for the wick capillary force by the aid of the validated new design technique.

5. Conclusions

An integrated TES with a 3 kW dish-Stirling engine was developed for a commercial CSP system. The basic functionality of the TES module was examined and verified by conducting various laboratory-scale tests on the system. The influence of the orientation of the TES module was determined by investigating the performance of the system in the vertical and horizontal orientations. The performance of the integrated system was better in the horizontal orientation than in the vertical setup, indicating the need for heat pipe refinement. The engine was able to maintain a 1 kW output while extracting stored energy from the PCM, implying that despite the low thermal conductivity of the solid PCM, the heat pipes were able to effectively withdraw thermal energy during the duration of the solidification process. The results have demonstrated that integrating a passive TES system with a dish-Stirling engine is feasible despite the underperformance of the current heat pipe design. Therefore, with further refinement and improvement of the heat pipe design, the TES system performance will be highly improved and can be used to decrease the LCOE associated with CSP plants.

Acknowledgments: This project was financially supported by DOE EERE. Majority of the development work was performed at Infinia Corporation by Ross Galbraith under the guidance of Songgang Qiu.

Author Contributions: Songgang Qiu conceived, designed, and performed the analytical analysis and experimental testing of the system. Songgang Qiu, Laura Solomon and Garrett Rinker analyzed the data and wrote the paper.

Conflicts of Interest: The authors declare no conflict of interest.

Nomenclature

CSP	Concentrating solar power
HTF	Heat transfer fluid
PCM	Phase change material
TES	Thermal energy storage
LCOE	Levelized cost of energy

References

1. Herrmann, U.; Kearney, D.W. Survey of Thermal Energy Storage for Parabolic Trough Power Plants. *J. Sol. Energy Eng.* **2002**, *124*, 145–152. [CrossRef]
2. Gil, A.; Medrano, M.; Martorell, I.; Lazaro, A.; Dolado, P.; Zalba, B.; Cabeza, L.F. State of the art on high temperature thermal energy storage for power generation. Part 1—Concepts, materials and modellization. *Renew. Sustain. Energy Rev.* **2010**, *14*, 31–55. [CrossRef]
3. Kuravi, S.; Trahan, J.; Goswami, D.Y.; Rahman, M.M.; Stefanakos, E.K. Thermal energy storage technologies and systems for concentrating solar power plants. *Prog. Energy Combust. Sci.* **2013**, *39*, 285–319. [CrossRef]
4. Stine, W.B.; Diver, R.B. *A Compendium of Solar Dish/Stirling Technology*; No. SAND93-7026; Sandia National Labs: Albuquerque, NM, USA, 1994.
5. Zheng, Y.; Zhao, W.; Sabol, J.C.; Tuzla, K.; Neti, S.; Oztekin, A.; Chen, J.C. Encapsulated phase change materials for energy storage—Characterization by calorimetry. *Sol. Energy* **2013**, *87*, 117–126. [CrossRef]
6. Zhao, W.; Zheng, Y.; Sabol, J.C.; Tuzla, K.; Neti, S.; Oztekin, A.; Chen, J.C. High temperature calorimetry and use of magnesium chloride for thermal energy storage. *Renew. Energy* **2013**, *50*, 988–993. [CrossRef]
7. Solomon, L.; Oztekin, A.; Neti, S.; Jain, H.; Pfeifer, T.; Matyáš, J.; Balaya, P.; Singh, D.; Wei, J. Determination of Parameters for Improved Efficiency in Thermal Energy Storage Using Encapsulated Phase Change Materials. In *Ceramics for Energy Conversion, Storage, and Distribution Systems*; John Wiley & Sons, Inc.: New York, NY, USA, 2016; pp. 219–226.
8. Singh, D.; Zhao, W.; Yu, W.; France, D.M.; Kim, T. Analysis of a graphite foam–NaCl latent heat storage system for supercritical CO2 power cycles for concentrated solar power. *Sol. Energy* **2015**, *118*, 232–242. [CrossRef]
9. Thapa, S.; Chukwu, S.; Khaliq, A.; Weiss, L. Fabrication and analysis of small-scale thermal energy storage with conductivity enhancement. *Energy Convers. Manag.* **2014**, *79*, 161–170. [CrossRef]
10. Almajali, M.; Lafdi, K.; Prodhomme, P.H. Effect of copper coating on infiltrated PCM/foam. *Energy Convers. Manag.* **2013**, *66*, 336–342. [CrossRef]
11. Kim, T.; France, D.M.; Yu, W.; Zhao, W.; Singh, D. Heat transfer analysis of a latent heat thermal energy storage system using graphite foam for concentrated solar power. *Sol. Energy* **2014**, *103*, 438–447. [CrossRef]
12. Zhao, C.Y.; Wu, Z.G. Heat transfer enhancement of high temperature thermal energy storage using metal foams and expanded graphite. *Sol. Energy Mater. Sol. Cells* **2011**, *95*, 636–643. [CrossRef]
13. Baby, R.; Balaji, C. Experimental investigations on thermal performance enhancement and effect of orientation on porous matrix filled PCM based heat sink. *Int. Commun. Heat Mass Transf.* **2013**, *46*, 27–30. [CrossRef]
14. Peiró, G.; Gasia, J.; Miró, L.; Cabeza, L.F. Experimental evaluation at pilot plant scale of multiple PCMs (cascaded) vs. single PCM configuration for thermal energy storage. *Renew. Energy* **2015**, *83*, 729–736. [CrossRef]
15. Shabgard, H.; Robak, C.W.; Bergman, T.L.; Faghri, A. Heat transfer and exergy analysis of cascaded latent heat storage with gravity-assisted heat pipes for concentrating solar power applications. *Sol. Energy* **2012**, *86*, 816–830. [CrossRef]
16. Solomon, L.; Oztekin, A. Exergy analysis of cascaded encapsulated phase change material—High-temperature thermal energy storage systems. *J. Energy Storage* **2016**, *8*, 12–26. [CrossRef]
17. Alam, T.E.; Dhau, J.S.; Goswami, D.Y.; Stefanakos, E. Macroencapsulation and characterization of phase change materials for latent heat thermal energy storage systems. *Appl. Energy* **2015**, *154*, 92–101. [CrossRef]
18. Jacob, R.; Bruno, F. Review on shell materials used in the encapsulation of phase change materials for high temperature thermal energy storage. *Renew. Sustain. Energy Rev.* **2015**, *48*, 79–87. [CrossRef]
19. Xu, B.; Li, P.; Chan, C. Application of phase change materials for thermal energy storage in concentrated solar thermal power plants: A review to recent developments. *Appl. Energy* **2015**, *160*, 286–307. [CrossRef]
20. Elmozughi, A.F.; Solomon, L.; Oztekin, A.; Neti, S. Encapsulated phase change material for high temperature thermal energy storage—Heat transfer analysis. *Int. J. Heat Mass Transf.* **2014**, *78*, 1135–1144. [CrossRef]
21. Solomon, L.; Elmozughi, A.F.; Neti, S.; Oztekin, A. High Temperature Thermal Energy Storage Using EPCM: The Effect of Void. In Proceedings of the ASME 2014 International Mechanical Engineering Congress and Exposition, Montreal, QC, Canada, 14–20 November 2014; American Society of Mechanical Engineers: Montreal, QC, Canada, 2014.

22. Solomon, L.; Elmozughi, A.F.; Oztekin, A.; Neti, S. Effect of internal void placement on the heat transfer performance–Encapsulated phase change material for energy storage. *Renew. Energy* **2015**, *78*, 438–447. [CrossRef]
23. Solomon, L.; Oztekin, A. Encapsulated Phase Change Materials for use in High Temperature Thermal Energy Storage. In *Advances in Energy Research*; Acosta, M.J., Ed.; Nova Science Publishers Inc.: Hauppauge, NY, USA, 2016.
24. Zhao, W.; Zheng, Y.; Sabol, J.C.; Oztekin, A.; Neti, S.; Tuzla, K.; Misiolek, W.M.; Chen, J.C. Heat Transfer Analysis for Thermal Energy Storage Using $NaNO_3$ as Encapsulated Phase Change Material. In Proceedings of the ASME 2012 Heat Transfer Summer Conference collocated with the ASME 2012 Fluids Engineering Division Summer Meeting and the ASME 2012 10th International Conference on Nanochannels, Microchannels, and Minichannels, Rio Grande, PR, USA, 8–12 July 2012; pp. 241–248.
25. Zheng, Y.; Barton, J.L.; Tuzla, K.; Chen, J.C.; Neti, S.; Oztekin, A.; Misiolek, W.Z. Experimental and computational study of thermal energy storage with encapsulated $NaNO_3$ for high temperature applications. *Sol. Energy* **2015**, *115*, 180–194. [CrossRef]
26. Liu, M.; Saman, W.; Bruno, F. Review on storage materials and thermal performance enhancement techniques for high temperature phase change thermal storage systems. *Renew. Sustain. Energy Rev.* **2012**, *16*, 2118–2132. [CrossRef]
27. Sharifi, N.; Bergman, T.L.; Faghri, A. Enhancement of PCM melting in enclosures with horizontally-finned internal surfaces. *Int. J. Heat Mass Transf.* **2011**, *54*, 4182–4192. [CrossRef]
28. Mat, S.; Al-Abidi, A.A.; Sopian, K.; Sulaiman, M.Y.; Mohammad, A.T. Enhance heat transfer for PCM melting in triplex tube with internal–external fins. *Energy Convers. Manag.* **2013**, *74*, 223–236. [CrossRef]
29. Hosseini, M.J.; Ranjbar, A.A.; Rahimi, M.; Bahrampoury, R. Experimental and numerical evaluation of longitudinally finned latent heat thermal storage systems. *Energy Build.* **2015**, *99*, 263–272. [CrossRef]
30. Shabgard, H.; Allen, M.J.; Sharifi, N.; Benn, S.P.; Faghri, A.; Bergman, T.L. Heat pipe heat exchangers and heat sinks: Opportunities, challenges, applications, analysis, and state of the art. *Int. J. Heat Mass Transf.* **2015**, *89*, 138–158. [CrossRef]
31. Naghavi, M.S.; Ong, K.S.; Mehrali, M.; Badruddin, I.A.; Metselaar, H.S.C. A state-of-the-art review on hybrid heat pipe latent heat storage systems. *Energy Convers. Manag.* **2015**, *105*, 1178–1204. [CrossRef]
32. Sharifi, N.; Wang, S.; Bergman, T.L.; Faghri, A. Heat pipe-assisted melting of a phase change material. *Int. J. Heat Mass Transf.* **2012**, *55*, 3458–3469. [CrossRef]
33. Motahar, S.; Khodabandeh, R. Experimental study on the melting and solidification of a phase change material enhanced by heat pipe. *Int. Commun. Heat Mass Transf.* **2016**, *73*, 1–6. [CrossRef]
34. Robak, C.W.; Bergman, T.L.; Faghri, A. Enhancement of latent heat energy storage using embedded heat pipes. *Int. J. Heat Mass Transf.* **2011**, *54*, 3476–3484. [CrossRef]
35. Shabgard, H.; Bergman, T.L.; Sharifi, N.; Faghri, A. High temperature latent heat thermal energy storage using heat pipes. *Int. J. Heat Mass Transf.* **2010**, *53*, 2979–2988. [CrossRef]
36. Tiari, S.; Qiu, S.; Mahdavi, M. Numerical study of finned heat pipe-assisted thermal energy storage system with high temperature phase change material. *Energy Convers. Manag.* **2015**, *89*, 833–842. [CrossRef]
37. Tiari, S.; Qiu, S.; Mahdavi, M. Discharging process of a finned heat pipe–assisted thermal energy storage system with high temperature phase change material. *Energy Convers. Manag.* **2016**, *118*, 426–437. [CrossRef]
38. Tiari, S.; Qiu, S. Three-dimensional simulation of high temperature latent heat thermal energy storage system assisted by finned heat pipes. *Energy Convers. Manag.* **2015**, *105*, 260–271. [CrossRef]
39. Hays, A.; Borquist, E.; Bailey, D.; Wood, D.; Weiss, L. Small-Scale Thermal Energy Storage with Capillary Conductivity Enhancement. In Proceedings of the ASME 2016 10th International Conference on Energy Sustainability Collocated with the ASME 2016 Power Conference and the ASME 2016 14th International Conference on Fuel Cell Science, Engineering and Technology, Charlotte, NC, USA, 26–30 June 2016.
40. Shabgard, H.; Faghri, A.; Bergman, T.L.; Andraka, C.E. Numerical Simulation of Heat Pipe-Assisted Latent Heat Thermal Energy Storage Unit for Dish-Stirling Systems. *J. Sol. Energy Eng.* **2013**, *136*, 021025. [CrossRef]
41. Sharifi, N.; Faghri, A.; Bergman, T.L.; Andraka, C.E. Simulation of heat pipe-assisted latent heat thermal energy storage with simultaneous charging and discharging. *Int. J. Heat Mass Transf.* **2015**, *80*, 170–179. [CrossRef]
42. Cui, H.; Wang, Z.; Guo, Y.; Xu, W.; Yuan, X. Thermal performance analysis on unit tube for heat pipe receiver. *Sol. Energy* **2006**, *80*, 875–882. [CrossRef]

43. Mahdavi, M.; Qiu, S.; Tiari, S. Numerical investigation of hydrodynamics and thermal performance of a specially configured heat pipe for high-temperature thermal energy storage systems. *Appl. Therm. Eng.* **2015**, *81*, 325–337. [CrossRef]
44. Mahdavi, M.; Qiu, S.; Tiari, S. Improvement of a novel heat pipe network designed for latent heat thermal energy storage systems. *Appl. Therm. Eng.* **2016**, *108*, 878–892. [CrossRef]
45. Mahdavi, M.; Qiu, S. Mathematical modeling and analysis of steady state performance of a heat pipe network. *Appl. Therm. Eng.* **2015**, *91*, 556–573. [CrossRef]